A first-principles study of Janus monolayer TiSSe and VSSe as anode materials in alkali metal ion batteries

Fen Xiong[1] and Yue Chen[1,2,*]

[1]Department of Mechanical Engineering, The University of Hong Kong, Pokfulam Road, Hong Kong SAR, China
[2]HKU Shenzhen Institute of Research and Innovation, Yuexing 2nd Road, Nanshan, Shenzhen 518057, China
*Corresponding author: yuechen@hku.hk

Abstract

Anode materials play an important role in the performance of rechargeable batteries and have been attracting much research interest. In this work, we have investigated the electrochemical properties of two dimensional (2D) Janus MSSe (M = Ti or V) for potential applications as anode materials in alkali metal ion batteries from density functional theory (DFT), following the recent successful synthesis of 2D Janus MoSSe. Our DFT calculations suggest that 2D Janus TiSSe and VSSe are stable in the 1T phase and 1H phase, respectively. It is found that alkali metal atoms X (X = Li, Na or K) can be stably adsorbed on the surfaces of Janus MSSe, and have low diffusion energy barriers. Additionally, small volume changes are observed in Janus MSSe after the adsorption of alkali metal atoms. It is predicted that the MSSe-2X systems have low open circuit voltages (OCVs) and high capacities. Our results suggest that 2D Janus TiSSe and VSSe are potential anode materials for alkali metal ion batteries.

Keywords: Janus TiSSe and VSSe; 2D materials; alkali metal ion battery

1. Introduction

Lithium-ion batteries are important energy storage systems, composed of anode, cathode and electrolyte. They are widely used in various digital devices and electric vehicles due to their high energy density and safety. With the miniaturization and lightweight of devices, Li-ion batteries are required to have higher energy density. To improve the energy storage capacity, the electrodes of Li-ion batteries have attracted significant research interest [1-3] and a variety of high-performance materials have been prepared as electrodes. For example, Wang et al. have synthesized Co_3O_4 nanospheres which can realize a 1455 $mAhg^{-1}$ capacity in Li-ion batteries [4]. Meanwhile, DFT calculations have predicted various promising electrode materials, including MXenes [5] and TMDs [6]. However, Li resource on earth is limited, so the cost of Li-ion batteries is affected by the price of Li. As Na and K elements have abundant resources and low cost, and their chemical properties are close to Li element, Na- and K-ion batteries have been considered as the alternatives of Li-ion batteries [7, 8]. Wu et al. have designed a low cost and environmentally friendly Na-ion battery based on $NaTi_2(PO_4)_3$–$Na_2NiFe(CN)_6$

[9].

Nanomaterials have been gaining research attention for their unparalleled behaviors over bulk materials. Their large specific surface area provides more adsorption sites for ions in batteries. Nanosized $LiMn_2O_4$ is demonstrated to have a higher storage capacity compared with microsized $LiMn_2O_4$ in Li-ion batteries [10]. The unique morphology of two-dimensional materials is beneficial for the diffusion of ions. The diffusion barriers of alkali metal atoms on GeS nanosheets are lower than those in bulk GeS [11]. With the decrease of thickness, the electrochemical properties of nanosheets may also be improved. Thinner nanosheets of Co_3O_4 exhibit better Li-ion diffusion performances due to shorter transport distances [12]. Many atomic-thick materials have been reported as excellent electrode materials. For example, the storage capacity of borophene monolayer is predicted to be as high as 1984 $mAhg^{-1}$ [13]; GaN monolayer has been reported as an excellent electrode material with high ion diffusion speed in Li- and Na-ion batteries [14].

Transition metal dichalcogenides (TMDs), layered materials with weak interlayer van der Waals (vdW) force, are widely used as photocatalysts [15], electrocatalysts [16] and supercapacitors [17]. As their layered structures are beneficial for the intercalation and diffusion of ions, they are promising electrode materials for rechargeable batteries. To improve their performance in batteries, a large number of methods have been reported [18], including surface defects [19] and alloying [20]. Defect-rich $MoS_{2(1-x)}Se_{2x}$ exhibits superior energy storage performance [21]. After the synthesis of MoS_2 nanosheets [22], two dimensional TMDs and their applications have received much research interest [23]. For example, MoS_2 monolayer is predicted to be a promising electrode material for alkali metal ion batteries [6, 24, 25]. Experimentally, TiS_2 [26] and VS_2 [27, 28] nanosheets are demonstrated to have high storage capacities in rechargeable batteries.

Recently, Lu et al. have synthesized a new two dimensional TMD, Janus MoSSe, by replacing the top-layer S atoms of MoS_2 monolayer with Se atoms [29]. With the inspiration of Janus MoSSe [30], more Janus TMDs have been proposed and most of them have been predicted to be dynamically stable, indicating that they may be synthesized in experiments [31-34]. For example, Janus WSSe monolayers have been successfully synthesized via the pulsed laser deposition technique [35]. Janus TiSC [36] and MoSSe [37-39] have been theoretically predicted to be promising electrode materials for rechargeable batteries. 1T-phase TiS_2 monolayer is a semiconductor and has been theoretically reported as an anode material for Na and K ion batteries [6, 25]. Motivated by Janus MoSSe,1T-phase Janus TiSSe monolayer has been proposed and is predicted to be metallic [40]. Generally, the electrochemical performances of materials are related to their electronic properties [41]; thus, 1T-phase TiSSe monolayer may exhibit different electrochemical behaviors from 1T-phase TiS_2 monolayer.

In this work, we have investigated the electrochemical performance of 2D Janus TiSSe and VSSe monolayer. Two crystal structures, 1T and 1H, have been considered. We

find that 1T-phase Janus TiSSe and 1H-phase Janus VSSe are energetically and dynamically stable. It is found that alkali metal atoms have large negative adsorption energies and low diffusion barriers on the surfaces of Janus TiSSe and VSSe. In addition, these Janus MSSe have small volume changes after the adsorption of alkali metal atoms, low OCVs and high specific capacities of up to approximately 330 $mAhg^{-1}$. Our calculations suggest that Janus TiSSe and VSSe are potential anode materials for alkali metal ion batteries.

2. Computational details

First-principles calculations were conducted using the Vienna Ab initio Simulation Package (VASP) [42]. The exchange-correlation effects were treated with the generalized gradient approximation of Perdew, Burke, and Ernzerhof [43]. The electronic wave functions were expanded using the plane wave basis set with a 350 eV cutoff energy. The convergence criterion for electrons was set to 10^{-5} eV. A *k*-point spacing of $2\pi \times 0.02$ $Å^{-1}$ was used to sample the Brillouin zone via the Γ-centered Monkhorst-Pack method. To model 2D materials, a vacuum space of approximately 15 Å was introduced along the *c* direction. A 9 × 9 × 1 supercell containing 243 atoms and a 1 × 1 × 1 *k*-mesh were applied to calculate the phonon dispersions using Phonopy [44] within density functional perturbation theory (DFPT). Dipole correction has also been considered.

3. Results and discussion

Two crystal structures of Janus TiSSe and VSSe have been considered in this work, including the 1T and 1H phases. As shown in Figure 1, both Janus crystal structures are composed of three layers of atoms; that is, a layer of transition metal atoms M (Ti or V) is located between the S and Se layers. To investigate their relative energetic stabilities, we have fully relaxed the two Janus crystal structures for TiSSe and VSSe to obtain their ground states. From our DFT calculations, the total energy differences ($\Delta E = E_{1T} - E_{1H}$) between the two Janus crystal structures are -370 and 42 meV for TiSSe and VSSe, respectively. It suggests that 1T phase of Janus TiSSe and 1H phase of Janus VSSe are more stable. To further study the dynamical stabilities of 1T-phase TiSSe and 1H-phase VSSe, we have calculated their phonon dispersions using Phonopy with the DFPT method, and the results are shown in Figure 1. It is seen that no imaginary phonons exist in 1T-phase TiSSe and 1H-phase VSSe, indicating that they are dynamically stable.

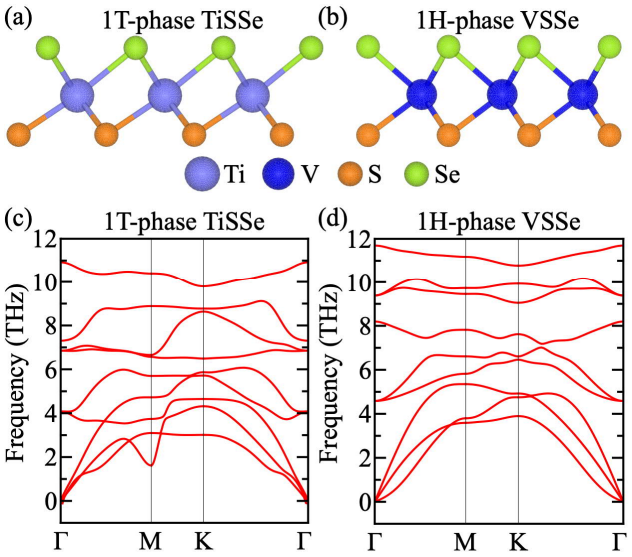

Figure 1. Crystal structures (a, b) and phonon dispersions (c, d) of 1T-phase Janus TiSSe and 1H-phase Janus VSSe.

To explore the potentials of 1T-phase Janus TiSSe and 1H-phase Janus VSSe as electrode materials in rechargeable batteries, we have constructed a 3 × 3 × 1 supercell containing 27 atoms to calculate the interactions between Janus TiSSe/VSSe and alkali metal atoms X (X = Li, Na or K). In order to identify the preferable adsorption sites of alkali metal atoms on the surfaces of 1T-phase TiSSe and 1H-phase VSSe, we have considered six possible adsorption sites, including the I^S/I^{Se}, II^S/II^{Se} and III^S/III^{Se} sites (see Figure 2). The adsorption energy is calculated with the following equation:

$$E_{ad} = E_{MSSe+X} - E_{MSSe} - E_X$$

where E_{MSSe+X}, E_{MSSe} and E_X represent the total energies of Janus MSSe adsorbed with an alkali metal atom, pristine Janus MSSe and an isolated alkali metal atom, respectively. It is observed from Figure 3 that alkali metal atoms can be stably adsorbed on both surfaces of MSSe, especially on the S surface. Heavier elements may have more negative adsorption energies. Alkali metal atoms generally prefer to be adsorbed at the I^S/II^{Se} site of TiSSe and the II^S/II^{Se} site of VSSe, except that K has a slightly lower energy when adsorbed at the III^{Se} site of TiSSe. When one alkali metal atom X is adsorbed on the S surface of Janus TiSSe, the adsorption energies at the I^S and II^S sites are very close, significantly lower than that at the III^S site. For the Se surface of TiSSe and both surfaces of VSSe, site I has the highest energies. It is noted that, when Na or K atom is adsorbed on the Se surface of TiSSe, the adsorption energies at the II and III sites almost overlap. When one K atom is adsorbed at the I^{Se} site, the crystal structure of TiSSe undergoes a large distortion; therefore, we have not considered this case in our discussion.

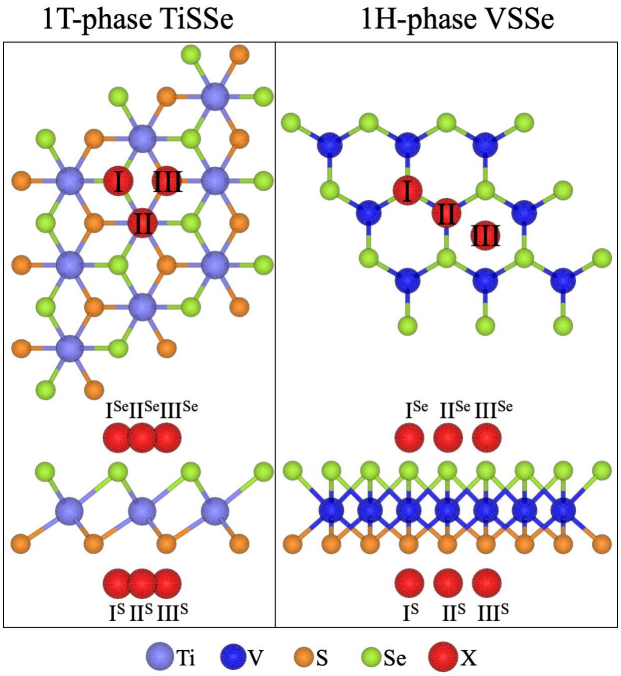

Figure 2. Top and side views of possible adsorption sites for 1T-phase Janus TiSSe and 1H-phase Janus VSSe. The superscripts S and Se represent the S and Se surfaces, respectively. The red spheres represent alkali metal atoms X (X = Li, Na or K).

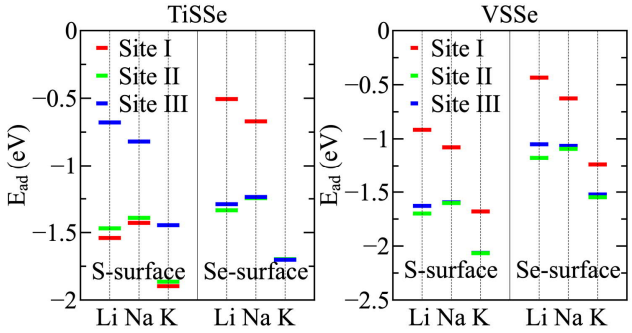

Figure 3. The adsorption energy of alkali metal atom X (X = Li, Na or K) at different sites on the S or Se surface of 3 × 3 × 1 supercells of TiSSe and VSSe.

To investigate the origin of the adsorption energy difference at different adsorption sites, we have compared the charge density differences when one Li atom is adsorbed at the I^S or III^S site of TiSSe (see Figure 4). Obvious charge transfer between the Li atom and the nearest S atoms can be observed in both cases. Nonetheless, when the Li atom is adsorbed at the I^S site, the Li atom has three nearest S atoms; when the Li atom is adsorbed at the III^S site, the Li atom only has one nearest S atom. These results rationalize that the Li atom on the S surface is more likely to adsorb at the I^S site due to the strong Li-S chemical bonds. In other cases, where the alkali metal atoms are adsorbed at their corresponding preferable sites, strong interactions are also found in-between the adsorbates and Janus MSSe (see Figure S1 and S2). Therefore, alkali metal atom X is predicted to be stably adsorbed on the surfaces of Janus TiSSe and VSSe with strong interactions.

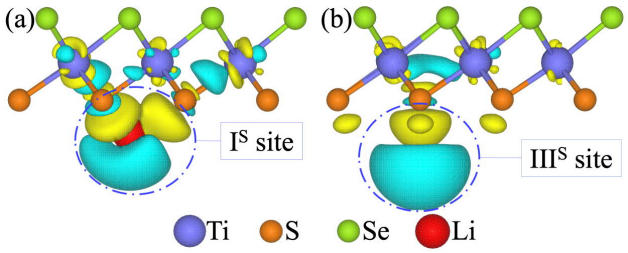

Figure 4. Charge density difference of TiSSe with Li adsorbed at the I^S or III^S site.

The charge-discharge rate is an important parameter to measure the performance of rechargeable batteries, which is mainly related to the diffusion behaviors of the working atoms on the electrode. To evaluate the diffusion abilities of alkali metal atoms on the surfaces of Janus TiSSe and VSSe, we have calculated their diffusion energy barriers between two nearest preferable adsorption sites via the climbing image nudged elastic band (CI-NEB) method (see Figure 5); the corresponding diffusion paths are shown in Figure S3 and S4. It is found that alkali metal atoms exhibit great diffusion performance. The diffusion energy barriers of alkali metal atoms Li, Na and K are 0.22/0.20, 0.14/0.11 and 0.10/0.07 eV on the S/Se surface of Janus TiSSe, and 0.20/0.22, 0.10/0.10 and 0.07/0.06 eV on the S/Se surface of Janus VSSe, respectively; these energy barriers are comparable to those on Janus MoSSe [38, 39].

The diffusion performances of alkali metal atoms on Janus TiSSe are similar to those on Janus VSSe. Although heavier alkali metal atoms may exhibit more stable adsorption, their diffusion performance can still be high on the surface of Janus MSSe; for example, the diffusion energy barriers of K are significantly lower than those of Na and Li. On the other hand, the alkali metal atoms on the Se surface have better diffusion performances than those on the S surface except VSSe with Li adsorption, for which the S surface has a lower diffusion barrier. When the K atom is adsorbed on the Se surface of Janus TiSSe, the energy of the transition state is slightly lower than that of the initial/final state, which may be related to the partial relaxation with fixed lattice in CI-NEB calculations. Therefore, it is predicted from our calculations that Janus TiSSe and VSSe may realize high charge-discharge rates in alkali metal ion batteries due to their relatively low diffusion barriers.

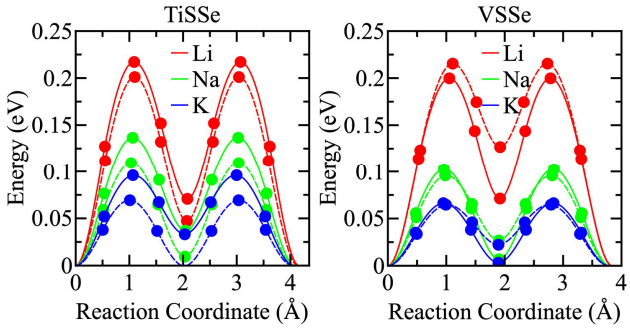

Figure 5. Diffusion-barrier profiles of alkali metal atoms between two nearest preferable adsorption sites of Janus TiSSe and VSSe. Solid and dashed curves represent

the S and Se surfaces, respectively.

In order to simulate high adsorption coverage for high storage capacity, we have modeled MSSe-2X systems based on a primitive cell of MSSe, in which one alkali metal atom X is adsorbed on the S surface and the other X is adsorbed on the Se surface. In our previous discussions, we have considered three possible adsorption sites on each surface. When each surface of MSSe is adsorbed by one alkali metal atom, there are nine possible adsorption configurations. To identify the most energetically stable adsorption configuration, we have fully relaxed the systems and calculated their total energies (see Table S3 and S4). It is found that most alkali metal atoms prefer the $I^{S}II^{Se}$ configuration in TiSSe and the $II^{S}II^{Se}$ configuration in VSSe, while K atoms tend to adsorb at the $III^{S}II^{Se}$ sites in VSSe. The intercalation/deintercalation of working atoms may lead to volume changes in the electrode, and a large volume change could result in the damage of electrode. Zhang et al. have suggested that the volume change of electrode should be lower than 25% [45]. We have compared the lattice constants of MSSe-2X before and after the adsorption of two alkali metal atoms, and the results are shown in Table 1. It is found that the changes of lattice constants caused by the adsorption of alkali metal atoms are relatively small, especially for Li and Na; for instance, the changes of in-plane lattice constants for MSSe-2Li and MSSe-2Na are below ~5%. Furthermore, the volume changes in TiSSe-2X are similar to those in VSSe-2X.

In addition to volume changes, open circuit voltage (OCV) and storage capacity are two important parameters to measure the performance of electrodes. To further investigate the potential applications of Janus TiSSe and VSSe in rechargeable batteries, we have calculated OCV and specific capacity for MSSe-2X systems (see Table 1). Open circuit voltages are calculated using the following equation [6]:

$$\mathrm{OCV} = (E_{MSSe} + nE_X - E_{MSSe+nX})/n$$

where $E_{MSSe+nX}$, E_{MSSe} and E_X represent the total energies of Janus MSSe adsorbed with X, pristine Janus MSSe and an isolated alkali-metal atom, respectively; and n is the number of adsorbed atoms. Generally, materials with an OCV lower than 1 eV may be used as anodes in alkali metal ion batteries [6]. It is found that all MSSe-2X systems have low OCVs in the range of 0.15-0.72 eV, and VSSe-2X has lower OCV compared with TiSSe-2X. The specific capacity is defined with the following formula [36]:

$$\mathrm{Capacity} = \frac{QF}{3.6 \times M_{\mathrm{MSSe}}}$$

where Q represents the number of electrons involved in the electrochemical process (for MSSe-2X, $Q = 2$); F is the Faraday constant; and M is the mass of MSSe in gmol^{-1}. The specific capacities of TiSSe-2X and VSSe-2X are approximately 337 and 331 mAhg^{-1}, respectively; these values are comparable to that of graphite (372 mAhg^{-1}), a commercialized anode material. The capacity of TiSSe-2X is close to that of VSSe-2X due to the similar chemical formula and mass.

Table 1. Theoretical structural parameters and OCVs of MSSe-2X in the most

energetically stable adsorption configuration; *a* represents the lattice constant along the *a* direction; *c* is the effective thickness of MSSe (distance between the S and Se layers plus their van der Waals radiuses); Δ*a* and Δ*c* are the corresponding changes after adsorption; *h* is the thickness of MSSe-2X (vertical distance between two X layers plus two times of its van der Waals radius).

Systems	*a* (Å)	Δ*a* (%)	*c* (Å)	Δ*c* (%)	h (Å)	OCV (V)
TiSSe-2Li ($I^{S}II^{Se}$)	3.65	5	6.76	1	8.80	0.72
VSSe-2Li ($II^{S}II^{Se}$)	3.40	4	6.73	-1	9.62	0.57
TiSSe-2Na ($I^{S}II^{Se}$)	3.61	4	6.67	0	11.33	0.43
VSSe-2Na ($II^{S}II^{Se}$)	3.40	5	6.67	-2	11.76	0.39
TiSSe-2K ($I^{S}II^{Se}$)	3.78	9	6.53	-2	12.77	0.33
VSSe-2K ($III^{S}II^{Se}$)	3.56	9	6.62	-2	13.14	0.15

4. Conclusions

The electrochemical properties of two-dimensional Janus TiSSe and VSSe have been investigated via first-principles calculations. The 1T phase of TiSSe and the 1H phase of VSSe are shown to be energetically and dynamically stable. It is found that alkali metal atoms can be stably adsorbed on Janus TiSSe and VSSe and have strong interactions with the substrates. Meanwhile, alkali metal atoms have relatively low diffusion energy barriers, indicating that they have good diffusion performance on the surfaces of Janus TiSSe and VSSe. On the other hand, under high ion coverage, Janus TiSSe and VSSe do not show significant volume changes and have high specific capacities and low open circuit voltages. Our findings may stimulate further experimental study of Janus monolayer TMDs as anode materials of alkali metal ion batteries.

Conflicts of interest

There are no conflicts of interest to declare.

Acknowledgments

This work is supported by the Research Grants Council of Hong Kong (17300018 and 17201019), the National Natural Science Foundation of China (11874313), the Science, Technology and Innovation Commission of Shenzhen Municipality (JCYJ20180307154619840), and the Environment and Conservation Fund (69/2018). The authors are grateful for the research computing facilities offered by ITS, HKU.

References

1. M. Li, J. Lu, Z. Chen and K. Amine, *Adv Mater*, 2018, **30**, 1800561.
2. A. P. Wang, S. Kadam, H. Li, S. Q. Shi and Y. Qi, *NPJ Comput Mater*, 2018, **4**, 1-26.
3. F. Zheng, M. Kotobuki, S. Song, M. O. Lai and L. Lu, *J Power Sources*, 2018, **389**, 198-213.
4. Y. Wang, R. Guo, W. Liu, L. Zhu, W. Huang, W. Wang and H. Zheng, *J Power*

Sources, 2019, **444**, 227260.
5. Q. Tang, Z. Zhou and P. Shen, *J Am Chem Soc*, 2012, **134**, 16909-16916.
6. E. Yang, H. Ji and Y. Jung, *J Phys Chem C*, 2015, **119**, 26374-26380.
7. P. K. Nayak, L. Yang, W. Brehm and P. Adelhelm, *Angew Chem Int Ed*, 2018, **57**, 102-120.
8. H. Kim, J. C. Kim, M. Bianchini, D. H. Seo, J. Rodriguez-Garcia and G. Ceder, *Adv Energy Mater*, 2018, **8**, 1702384.
9. X. Wu, Y. Cao, X. Ai, J. Qian and H. Yang, *Electrochem Commun*, 2013, **31**, 145-148.
10. Y. Chen, K. Xie, Y. Pan and C. Zheng, *J Power Sources*, 2011, **196**, 6493-6497.
11. F. Li, Y. Qu and M. Zhao, *J Mater Chem A*, 2016, **4**, 8905-8912.
12. J. Li, Z. Li, F. Ning, L. Zhou, R. Zhang, M. Shao and M. Wei, *ACS Omega*, 2018, **3**, 1675-1683.
13. X. Zhang, J. Hu, Y. Cheng, H. Y. Yang, Y. Yao and S. A. Yang, *Nanoscale*, 2016, **8**, 15340-15347.
14. X. Zhang, L. Jin, X. Dai, G. Chen and G. Liu, *ACS Appl Mater Interfaces*, 2018, **10**, 38978-38984.
15. Y. Chen, H. Sun and W. Peng, *Nanomaterials*, 2017, **7**, 62.
16. Q. Lu, Y. Yu, Q. Ma, B. Chen and H. Zhang, *Adv Mater*, 2016, **28**, 1917-1933.
17. R. N. A. R. Seman, M. A. Azam and M. H. Ani, *Nanotechnology*, 2018, **29**, 502001.
18. B. Chen, D. Chao, E. Liu, M. Jaroniec, N. Zhao and S.-Z. Qiao, *Energy Environ Sci*, 2020, **13**, 1096-1131.
19. X. Sun, Z. Wang and Y. Q. Fu, *Sci Rep*, 2015, **5**, 18712.
20. F. Ersan, G. k. Gökoğlu and E. Aktürk, *J Phys Chem C*, 2015, **119**, 28648-28653.
21. G. Cai, L. Peng, S. Ye, Y. Huang, G. Wang and X. Zhang, *J Mater Chem A*, 2019, **7**, 9837-9843.
22. K. F. Mak, C. Lee, J. Hone, J. Shan and T. F. Heinz, *Phys Rev Lett*, 2010, **105**, 136805.
23. J.-H. Liao, Y.-C. Zhao, Y.-J. Zhao, X.-B. Yang and Y. Chen, *J Appl Phys*, 2020, **127**, 044301.
24. G. Barik and S. Pal, *J Phys Chem C*, 2019, **123**, 21852-21865.
25. Z. Zhang, M. Yang, N. Zhao, L. Wang and Y. Li, *Phys Chem Chem Phys*, 2019, **21**, 23441-23446.
26. Z. Hu, Z. Tai, Q. Liu, S. W. Wang, H. Jin, S. Wang, W. Lai, M. Chen, L. Li and L. Chen, *Adv Energy Mater*, 2019, **9**, 1803210.
27. D. Yu, Q. Pang, Y. Gao, Y. Wei, C. Wang, G. Chen and F. Du, *Energy Storage Mater*, 2018, **11**, 1-7.
28. D. Wu, C. Wang, M. Wu, Y. Chao, P. He and J. Ma, *J Energy Chem*, 2020, **43**, 24-32.
29. A.-Y. Lu, H. Zhu, J. Xiao, C.-P. Chuu, Y. Han, M.-H. Chiu, C.-C. Cheng, C.-W. Yang, K.-H. Wei and Y. Yang, *Nat Nanotechnol*, 2017, **12**, 744-749.
30. J. Zhang, S. Jia, I. Kholmanov, L. Dong, D. Er, W. Chen, H. Guo, Z. Jin, V. B. Shenoy and L. Shi, *ACS Nano*, 2017, **11**, 8192-8198.

31. W. Shi and Z. Wang, *J Phys Condens Matter*, 2018, **30**, 215301.
32. Y. Cheng, Z. Zhu, M. Tahir and U. Schwingenschlögl, *EPL*, 2013, **102**, 57001.
33. W.-L. Tao, J.-Q. Lan, C.-E. Hu, Y. Cheng, J. Zhu and H.-Y. Geng, *J Appl Phys*, 2020, **127**, 035101.
34. W. Chen, X. Hou, X. Shi and H. Pan, *ACS Appl Mater Interfaces*, 2018, **10**, 35289-35295.
35. Y.-C. Lin, C. Liu, Y. Yu, E. Zarkadoula, M. Yoon, A. A. Puretzky, L. Liang, X. Kong, Y. Gu and A. Strasser, *ACS Nano*, 2020, **14**, 3896-3906.
36. W. Chen, Y. Qu, L. Yao, X. Hou, X. Shi and H. Pan, *J Mater Chem A*, 2018, **6**, 8021-8029.
37. S.-H. Zhou, J. Zhang, Z.-Z. Ren, J.-F. Gu, Y.-R. Ren, S. Huang, W. Lin, Y. Li, Y.-F. Zhang and W.-K. Chen, *Chem Phys*, 2020, **529**, 110583.
38. H. Wang, Q. Chen, H. Li, Q. Duan, D. Jiang and J. Hou, *Chem Phys Lett*, 2019, **735**, 136777.
39. C. Shang, X. Lei, B. Hou, M. Wu, B. Xu, G. Liu and C. Ouyang, *J Phys Chem C*, 2018, **122**, 23899-23909.
40. A. Mogulkoc, Y. Mogulkoc, S. Jahangirov and E. Durgun, *J Phys Chem C*, 2019, **123**, 29922-29931.
41. P. S. Kumar, S. Ayyasamy, E. S. Tok, S. Adams and M. Reddy, *ACS Omega*, 2018, **3**, 3036-3044.
42. G. Kresse and J. Furthmüller, *Phys Rev B*, **54**, 11169-11186.
43. J. P. Perdew, K. Burke and M. Ernzerhof, *Phys Rev Lett*, 1996, **77**, 3865.
44. A. Togo, F. Oba and I. Tanaka, *Phys Rev B*, 2008, **78**, 134106.
45. X. Zhang, Z. Zhang, S. Yao, A. Chen, X. Zhao and Z. Zhou, *Npj Comput Mater*, 2018, **4**, 1-6.